Effects of Aortic Root Motion on Wall Stress in the Marfan Aorta Before and After Personalised Aortic Root Support (PEARS) Surgery

S. D. Singh[a], X. Y. Xu[a,*], J. R. Pepper[b,c], C. Izgi[b], T. Treasure[d], R. H. Mohiaddin[b,c]

[a]Department of Chemical Engineering, Imperial College London, South Kensington Campus, London SW7 2AZ, UK

[b]Royal Brompton and Harefield NHS Foundation Trust, Sydney Street, London SW3 6NP, UK

[c]National Heart and Lung Institute, Imperial College London, London SW7 2AZ, UK

[d]Clinical Operational Research, University College London, Department of Mathematics, 4 Taviton Street, London WC1H 0BT, UK

* Corresponding author. Tel.: +44 (0)2075945588; Fax: +44 (0)2075941989; E-mail: yun.xu@imperial.ac.uk

Word count:

ABSTRACT

Aortic root motion was previously identified as a risk factor for aortic dissection due to increased longitudinal stresses in the ascending aorta. The aim of this study was to investigate the effects of aortic root motion on wall stress and strain in the ascending aorta and evaluate changes before and after implantation of personalised external aortic root support (PEARS).

Finite element (FE) models of the aortic root and thoracic aorta were developed using patient-specific geometries reconstructed from pre- and post-PEARS cardiovascular magnetic resonance (CMR) images in three Marfan patients. The wall and PEARS materials were assumed to be isotropic, incompressible and linearly elastic. A static load on the inner wall corresponding to the patients' pulse pressure was applied. Cardiovascular MR cine images were used to quantify aortic root motion, which was imposed at the aortic root boundary of the FE model, with zero-displacement constraints at the distal ends of the aortic branches and descending aorta.

Measurements of the systolic downward motion of the aortic root revealed a significant reduction in the axial displacement in all three patients post-PEARS compared with its pre-PEARS counterparts. Higher longitudinal stresses were observed in the ascending aorta when compared with models without the root motion. Implantation of PEARS reduced the longitudinal stresses in the ascending aorta by up to 52%. In contrast, the circumferential stresses at the interface between the supported and unsupported aorta were increase by up to 82%. However, all peak stresses were less than half the known yield stress for the dilated thoracic aorta.

Introduction

Acute aortic dissection is the most prevalent cause of death in patients with Marfan syndrome. Aortic wall abnormalities and aortic dilatation are known to influence mechanical stresses in the aortic wall and are the most common risk factors for aortic dissection and rupture (Beller et al., 2004). It is well-known that in most acute dissections of the ascending aorta there is a transverse intimal tear a few centimetres distal to the aorto-ventricular junction (Hirst et al., 1958). More recent studies have suggested that aortic root motion may be a factor for occurrence of dissection and the site of the intimal tear due to increased longitudinal wall stresses (Beller et al., 2004, Beller et al., 2008b).

Ventricular relaxation and contraction during every heartbeat provides a driving force for the downward movement of the aortic annulus, which is then transmitted to the aortic root, ascending aorta, transverse aortic arch and aortic branches. Beller et al. (2004) used aortograms to analyse the extent of aortic root motion in 40 patients with coronary artery heart disease. It was found that the peak downward axial displacement of the aortic root during a cardiac cycle ranged between 0% and 49% of the sinotubular junction (STJ) diameter, with a median of 14% (IQR 7% to 22%). Other cardiac pathology also affected aortic root movement, where patients with aortic insufficiency showed increased aortic root motion because of increased left ventricular stroke volume while patients with left ventricular systolic dysfunction displayed reduced aortic root motion because of reduced ventricular contraction.

Stress analysis of the thoracic aorta was then carried out to investigate the influence of aortic root motion on wall stress in the ascending aorta (Beller et al., 2004) and evaluate the risk of aortic dissection (Beller et al., 2008b). A finite element (FE) model of an average adult human aortic root (excluding the sinuses of Valsalva), aortic arch and aortic branches was constructed using measurements obtained from a silicone mould of a normal human aorta while the arch spatial orientation was obtained from 3D reconstruction of MR images of a healthy volunteer (Beller et al., 2008b). An 8.9 mm axial displacement was imposed at the aortic root base, followed by a 6° twist. These values were obtained from healthy volunteers in studies by Kozerke et al. (1999) (for displacement) and Stuber et al. (1999) (for twist). Key findings were that pressurisation alone did not appreciably deform the model, but including the axial displacement caused significant deformation to the ascending aorta and brachiocephalic trunk. In the control model (without aortic root motion), high stress concentrations were found at the ostia of the aortic arch branches. Upon addition of the aortic root motion, there were no marked change in circumferential or longitudinal stresses between these branches, but the longitudinal stress in the ascending aorta (approximately 2 cm above the STJ) increased by 50%. Furthermore, including the twist did not result in any appreciable changes in the deformation or longitudinal stresses.

In spite of the high stress concentrations at the ostia of the aortic arch branches, mechanical failures are not typically observed in these regions. However, increased longitudinal stress in the ascending aorta may render this region at increased risk of degeneration of the aortic media and intimal rupture (Beller et al., 2004, Beller et al., 2008b), especially in patients with a vulnerable aortic wall due to connective tissue disease. As an aortic aneurysm dilates, the longitudinal stress in the dilated region also increases significantly, and may result in rupture (Thubrikar et al., 1999). If located in the ascending aorta, aortic root motion may then result in an additional increase in the longitudinal stress of the aneurysm, consequently enhancing the risk of rupture of small aneurysms, which are not usually considered for surgery (Beller et al., 2008b). Furthermore, aortic root motion may dislodge atherosclerotic debris from the aortic wall, leading to stroke or other embolic events, or lead to accelerated degeneration of homografts, autografts and bioprosthetic valves (Beller et al., 2008b). Changes in the magnitude of aortic root motion before and after aortic valve replacement (AVR) was evaluated in patients with aortic insufficiency, aortic stenosis and proximal aortic dissection (Beller et al., 2008a). Postoperative aortic root motion was significantly reduced after AVR in patients with initial aortic insufficiency, while it was appreciably increased in patients with initial aortic stenosis. However, based on their findings from the FE study (Beller et al., 2004, Beller et al., 2008b), increased aortic root motion caused higher longitudinal wall stress, which may in turn have harmful consequences in the context of a thinned, post-stenotic, dilated aorta.

These findings form the underlying interest in the effect of aortic root motion on mechanical stresses in the Marfan aorta upon insertion of personalised external aortic root support (PEARS; ExoVasc®, Exstent Ltd, Tewkesbury, UK) (Treasure et al., 2011). Follow-up cardiovascular magnetic resonance (CMR) imaging studies of the aortic root upon insertion of PEARS revealed that in addition to preventing further dilatation (Pepper et al., 2010a, Pepper et al., 2010b), the stiffer PEARS also caused a reduction in the aortic root motion (Izgi et al., 2015). In a previous study, FE models were developed to compare the stress and strain fields in Marfan aortas pre- and post-PEARS implantation, where one of the assumptions made was zero-displacement at the aortic root (Singh et al., 2015). The present study investigates the effects of aortic root motion on wall stress and strain in patient-specific Marfan aortas before and after implantation of PEARS.

Methods

Patient-Specific Geometry

MR images before and after implantation of PEARS were obtained (see Table 1 for imaging parameters). These were used to reconstruct patient-specific models of the aorta using Mimics (Materialise, Louvain, Belgium).

Table 1: Magnetic resonance imaging parameters for Patients 1, 2 and 3

		Repetition time (ms)	Echo time (ms)	Flip angle (°)	Pixel size (mm)	Slice thickness (mm)	Interslice distance (mm)	Image frequency (MHz)
Patient 1	Pre	292.10	1.22	80	1.328	6.0	3	63.67
	Post	296.38	1.07	70	0.594	1.5	var.	63.67
Patient 2	Pre	221.00	1.40	90	0.781	0.8	0.8	63.68
	Post	251.00	1.45	70	0.625	2.0	2.0	63.68
Patient 3	Pre	338.87	1.22	80	1.328	6.0	3.0	63.68
	Post	292.10	1.22	80	1.328	6.0	3.0	63.68

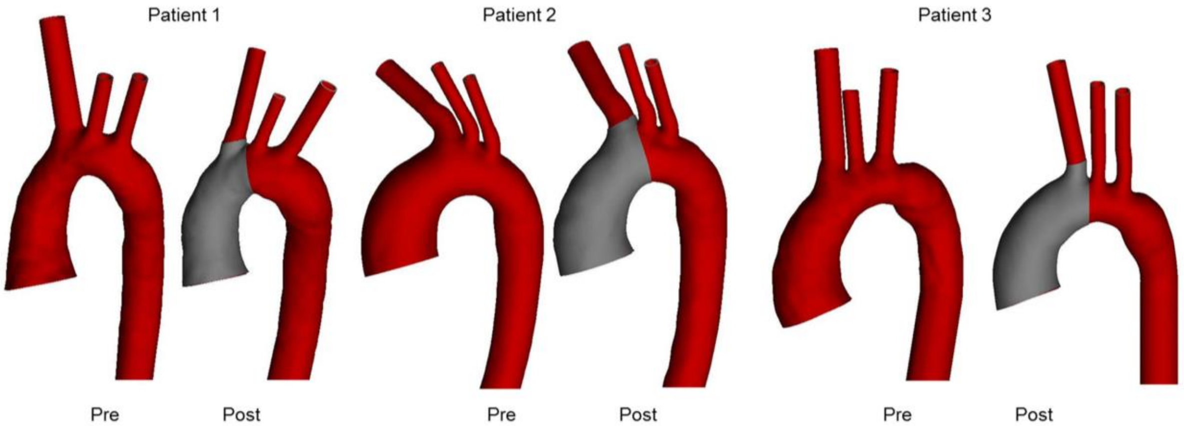

Figure 1: Reconstructed patient-specific geometries for Patients 1, 2 and 3 before and after implementation of PEARS

A uniform wall thickness was assumed for each aorta; the post-PEARS wall was thicker to account for the formation of a periarterial fibrotic sheet (Verbrugghe et al., 2013). The aortic branches were assumed to have the same thickness as the aorta. ANSYS ICEM CFD (ANSYS, Canonsburg, PA, USA) was used to discretise the resulting geometries using hexahedral elements. Mesh independence tests were performed using mesh sizes of 1.0×10^5, 2.5×10^5 and 5.0×10^5 elements. The differences in terms of peak displacement, peak stress and peak strain were less than 1.5% between the 1.0×10^5 element mesh and the 2.5×10^5 element mesh and less than 1.0% between the 2.5×10^5 and 5.0×10^5 element mesh. Computational time deficit was negligible in all cases, as each simulation was completed within 3 hours. Consequently, the number of elements used was between 2.5×10^5 and 5.0×10^5 elements.

Assessment of Aortic Root Motion

The aortic root motion was defined as the systolic downward motion of the aortic valve annulus. The left ventricular outflow tract cross-cut (LVOTxc) CMR cine images were used to identify the aortic valve annular plane in diastole and systole. These two planes were not parallel to each other due to the three-dimensional motion of the aortic root. Therefore, the systolic downward motion was measured as the length of the perpendicular line connecting the mid-point of the diastolic annulus plane and its intersection with the systolic annulus plane (see Figure 2) (Izgi 2015).

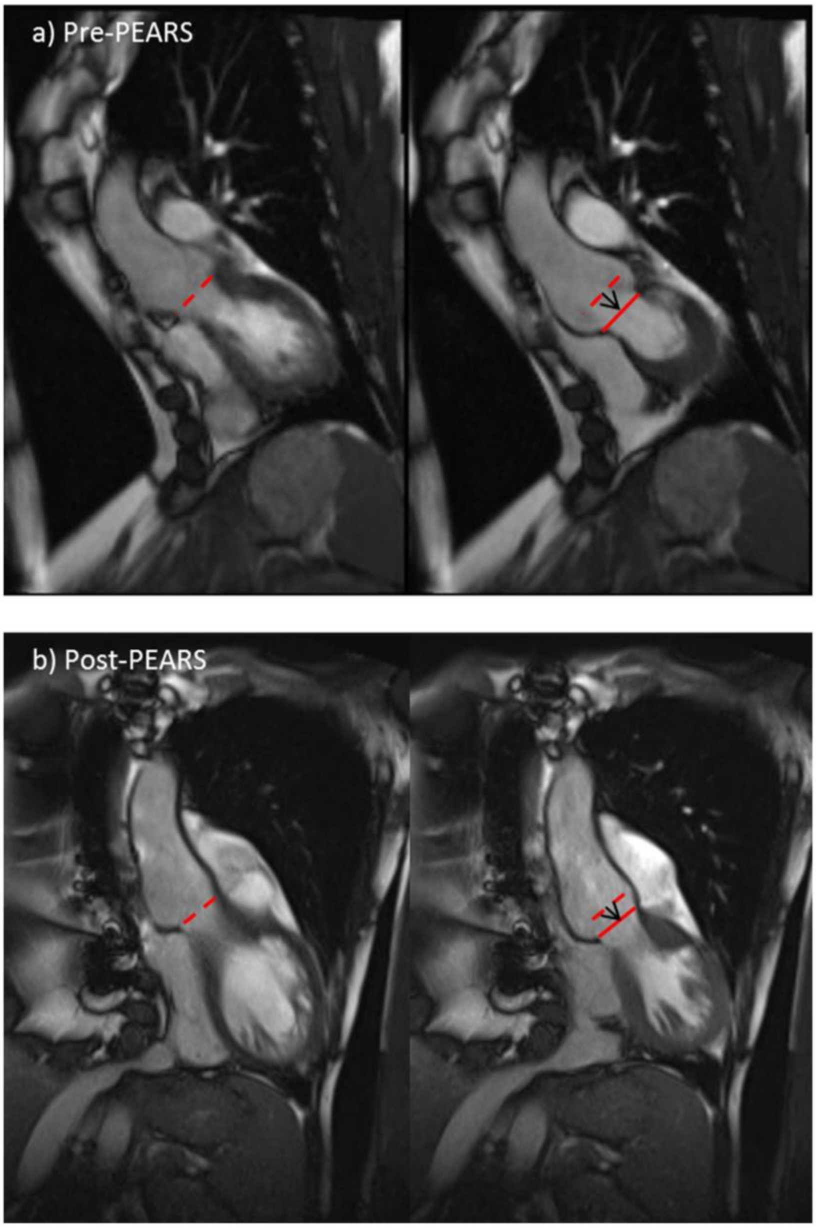

Figure 2: Measurement of the systolic downward aortic root motion (in Patient 1) for the (a) pre-PEARS aorta and (b) post-PEARS aorta. The annular plane at end-diastole is illustrated by the dashed line, while the plane at end-systole is illustrated by the solid line. The aortic root motion is quantified as the length of the perpendicular line connecting the mid-point of each annular plane

Material Properties

The aortic wall was modelled using a linear elastic constitutive equation, assuming it to be incompressible, homogenous and isotropic. It was assumed that the aortic branches had the same properties as the pre-PEARS aorta. The material properties are summarised in Table 2.

The justification for the choice of material properties for the post-PEARS material can be found in our previous work (Singh et al., 2015).

Table 2: Wall material properties used in the finite element models

	Pre-PEARS	Post-PEARS
Elastic modulus (kPa)	3000	6750
Poisson's ratio	0.49	0.45
Wall thickness (mm)	1.0	1.5
References	Nathan et al. (2011)	Verbrugghe et al. (2013)

Boundary Conditions

A static load corresponding to the patients' pulse pressure (see Table 3) was applied perpendicular to the inner surface of the aorta. At the aortic root, an axial downward motion was specified based on the measurements obtained for each patient. Zero-displacement constraints were set at the distal ends of the brachiocephalic, left common carotid and left subclavian arteries, and in the mid-descending aorta.

Table 3: Patient data used in this study

	Patient 1		Patient 2		Patient 3	
	Pre	Post	Pre	Post	Pre	Post
Blood Pressure (mmHg)						
Systolic	135	130	110	110	118	110
Diastolic	78	70	60	60	84	70
Pulse	57	60	50	50	34	40

ANSYS Mechanical (ANSYS, Canonsburg, PA, USA) was employed to obtain numerical solutions. Large-displacement (non-linear) static analyses were performed with the pressure and displacement loads ramped over several sub-steps. A preconditioned conjugate gradient (PCG) solver was selected and convergence was controlled by defining a square-root-sum-of-squares (SRSS) residual of 10^{-8}, which was achieved within 6-12 iterations. Simulations were performed using a 16.0 GB RAM personal computer with Intel® Core™ i7-2600 3.40 GHz, running Windows 7 Enterprise.

Results

Aortic Root Motion

The systolic downward motion of the aortic root in all three patients, pre- and post-PEARS implantation was measured and the results are given in Table 4. It shows clearly that PEARS implantation significantly reduced the axial root displacement in all three patients.

Table 4: Downward systolic aortic root motion measurements

	Aortic Root Motion (mm)	
	Pre-PEARS	Post-PEARS
Patient 1	15.5	8.3
Patient 2	15.7	8.3
Patient 3	10.5	7.0

This is consistent with the study by Izgi et al. (2015) who examined a cohort of 24 patients (pre- and post-PEARS) and reported that the average systolic downward motion of the aortic root prior to implantation of PEARS was 12.6±3.6 mm while after implantation, it decreased to 7.9±2.9 mm.

Deformation

In all the models, introduction of the aortic root motion resulted in significantly greater deformation of the aorta compared to pressurisation alone, as shown in Figure 3. **Error! Reference source not found.** highlights the changes in spatial distributions of displacements in each aorta. Without aortic root motion, peak displacements in the pre-PEARS and post-PEARS models were found at different locations: these were in the proximal ascending aorta and around the aortic arch pre-PEARS, but in the descending aorta post-PEARS. Upon introduction of root motion, peak displacements were shifted to the moving aortic root boundary. The general trends can be summarised as follows:

- Post-PEARS models showed a reduction in maximum displacement when compared with its pre-PEARS counterparts, with and without aortic root motion; and
- Including aortic root motion resulted in significant increases in peak displacement in all models.

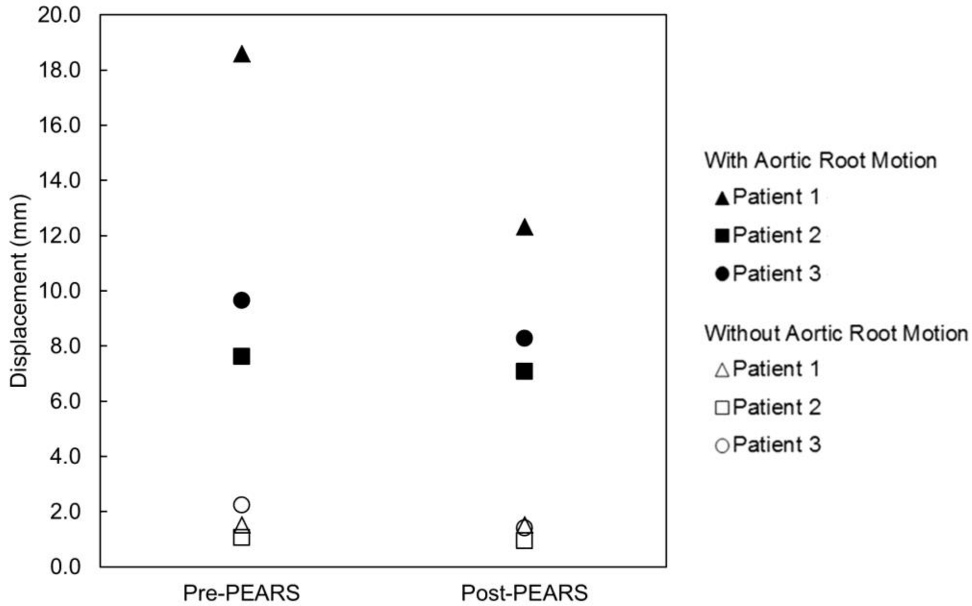

Figure 3: Peak displacement observed in the pre- and post-PEARS models with and without aortic root motion

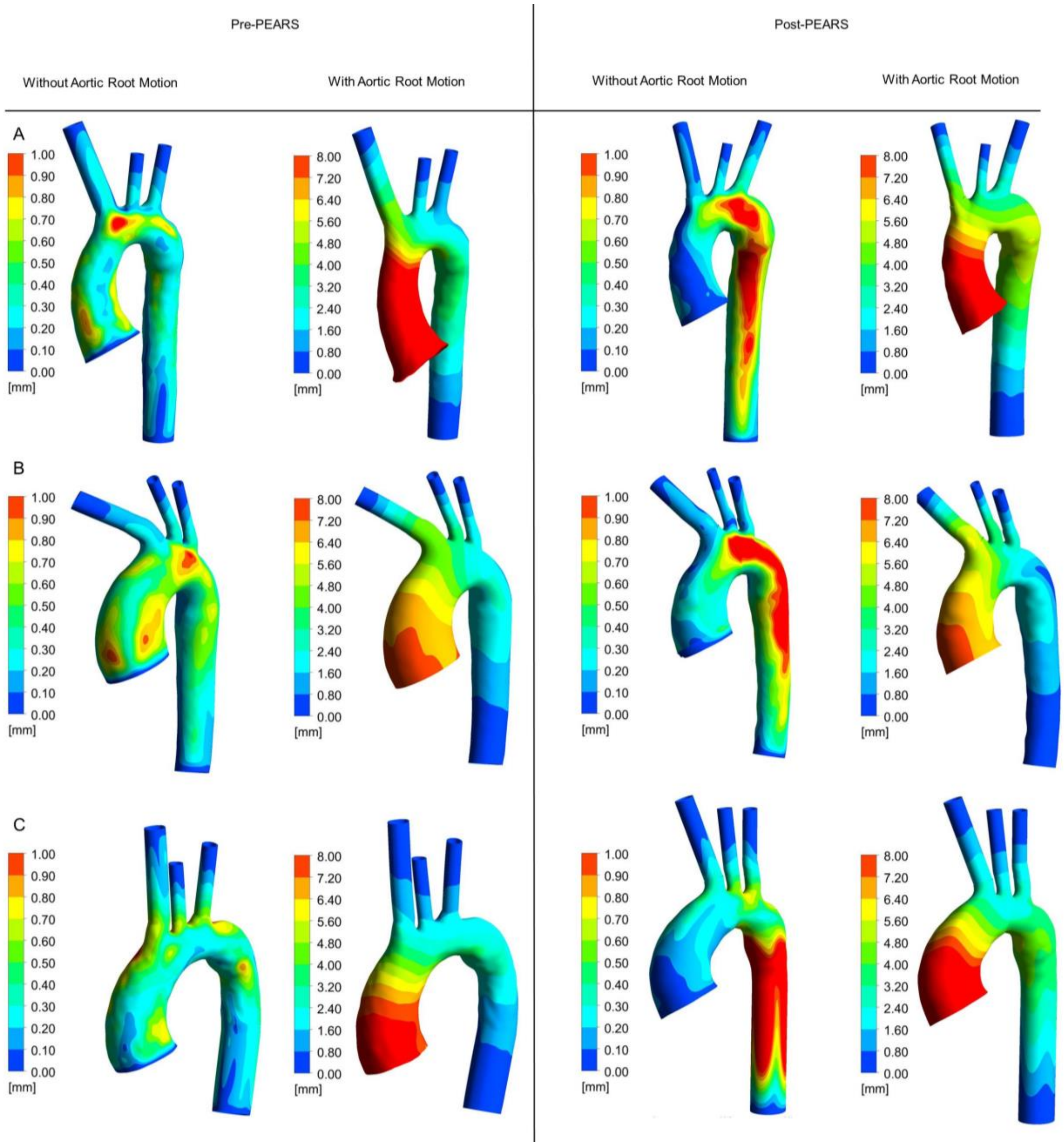

Figure 4: Displacement contours in the pre- and post-PEARS models with and without aortic root motion (A: Patient 1; B: Patient 2; C: Patient 3). Note the models with and without aortic root motion are displayed using different colour maps; the models without aortic root motion are illustrated with a maximum displacement (red) of 1 mm while the models with aortic root motion are illustrated with a maximum displacement (red) of 8 mm.

Stresses without Aortic Root Motion

Without aortic root motion, the pre-PEARS models displayed higher longitudinal and circumferential stresses in the proximal ascending aorta compared with the post-PEARS models, as shown in Figure 5 and Figure 6. The high longitudinal and circumferential stress regions in the post-PEARS were located at the interface between the supported and unsupported aorta (between the BCA and the left common carotid artery (LCCA)) and regions distal to this interface.

Stresses with Aortic Root Motion

It can immediately be recognised from Figure 5 that the aortic root motion resulted in higher longitudinal stresses, particularly in the pre-PEARS models. The stiffer post-PEARS models, on the other hand, experienced slightly more conservative increases. Additionally, elevated longitudinal stress in the ascending aorta was located at the inner curvature and then extended to the outer curvature proximal to the brachiocephalic trunk. Circumferential stress distributions, shown in Figure 6, with and without aortic root motion, are quite similar. Unlike the longitudinal stress patterns, high circumferential stress regions were found mostly on the outer curvature of the ascending aorta. The absolute values of the changes in circumferential and longitudinal stresses at two specific regions, with and without aortic root motion, for all models are shown in **Error! Reference source not found.**. Since each model was constructed using patient-specific geometries and loadings, the quantitative results were different among the patients. However, the qualitative effects of aortic root motion are quite similar and these are summarised as follows:

- Circumferential stress between the BCA and LCCA: this was reduced in all models, except for the pre-PEARS model of Patient 2 which showed an increase;
- Circumferential stress in the proximal ascending aorta: no change was observed in the pre-PEARS models of Patients 1 and 2, while Patient 3 showed a 25% decrease; in the post-PEARS, all models showed increased circumferential stress in this region;

- Longitudinal stress between the BCA and LCCA: a significant increase was observed in the pre- and post-PEARS models of Patient 2 and 3, while Patient 1 displayed a modest increase;
- Longitudinal stress in the proximal ascending aorta: again, all models showed significant increases.

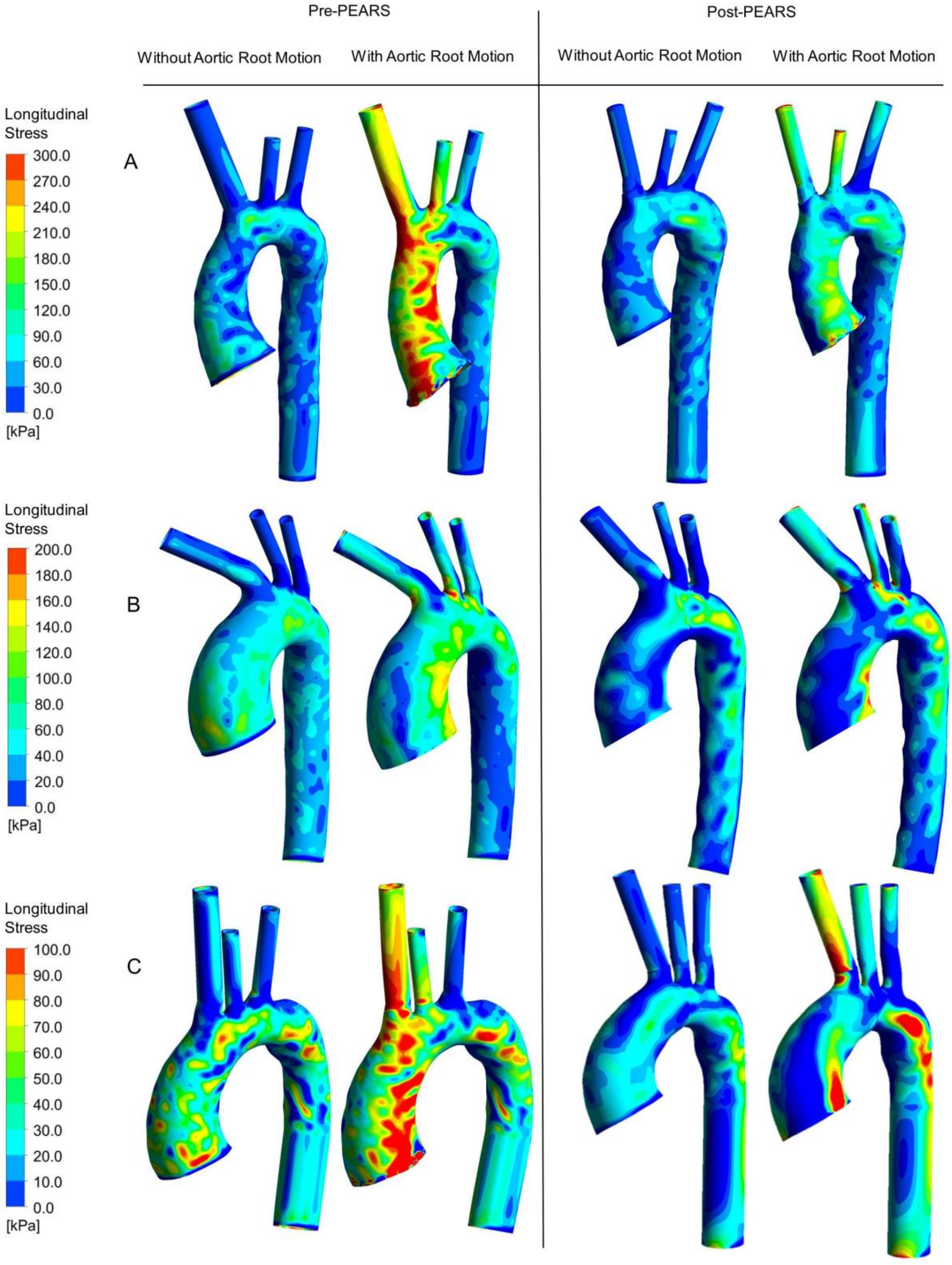

Figure 5: Longitudinal stress contour plots for the pre- and post-PEARS models of Patients 1, 2 and 3 (labelled A, B and C, respectively), with and without aortic root motion. Note that each patient is illustrated using a different contour colour map scale owing to differences in biomechanical properties

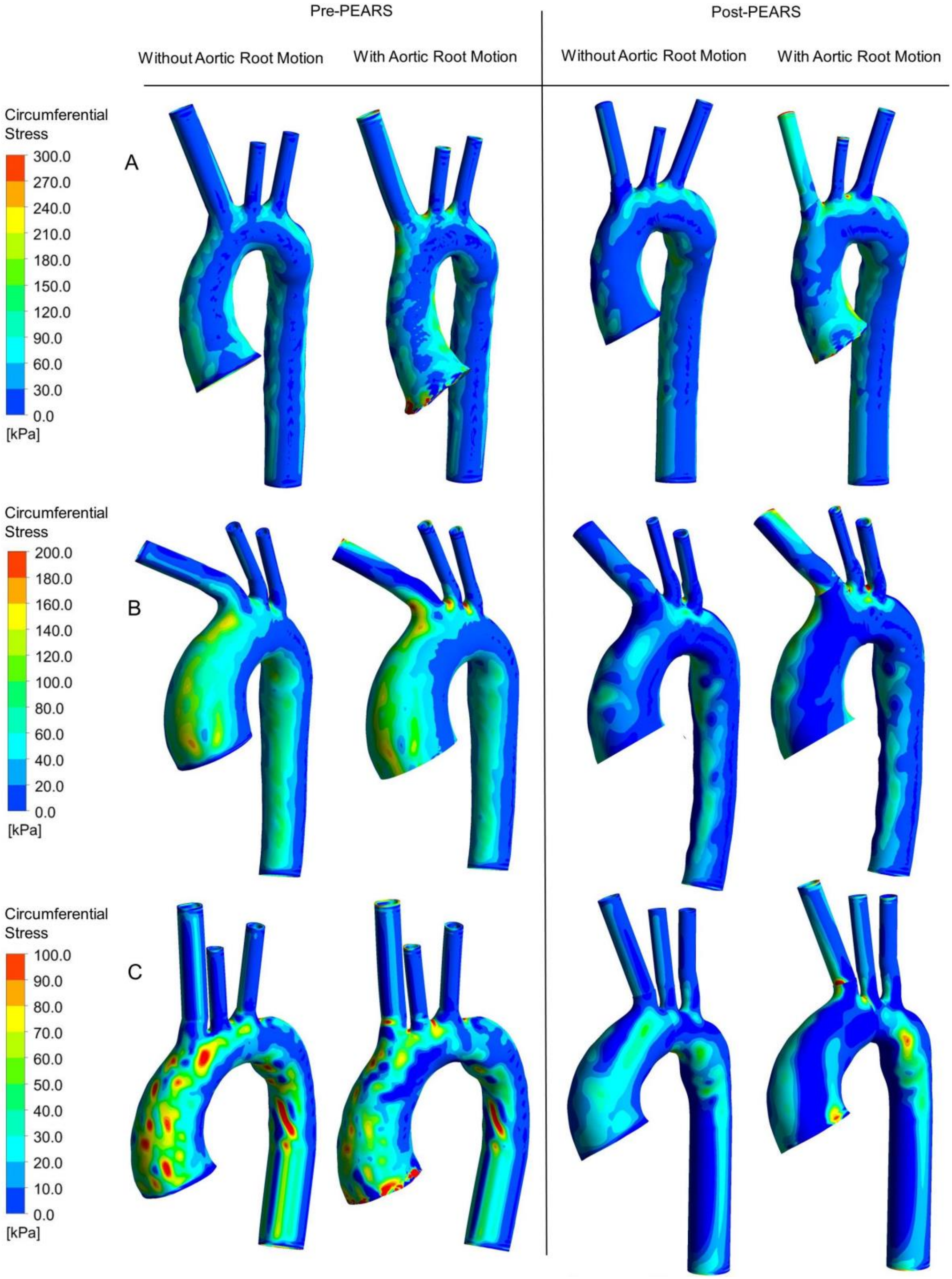

Figure 6: Circumferential stress contour plots for the pre- and post-PEARS models of Patients 1, 2 and 3 (labelled A, B and C, respectively), with and without aortic root motion. Note that each patient is illustrated using a different contour colour map scale owing to differences in biomechanical properties

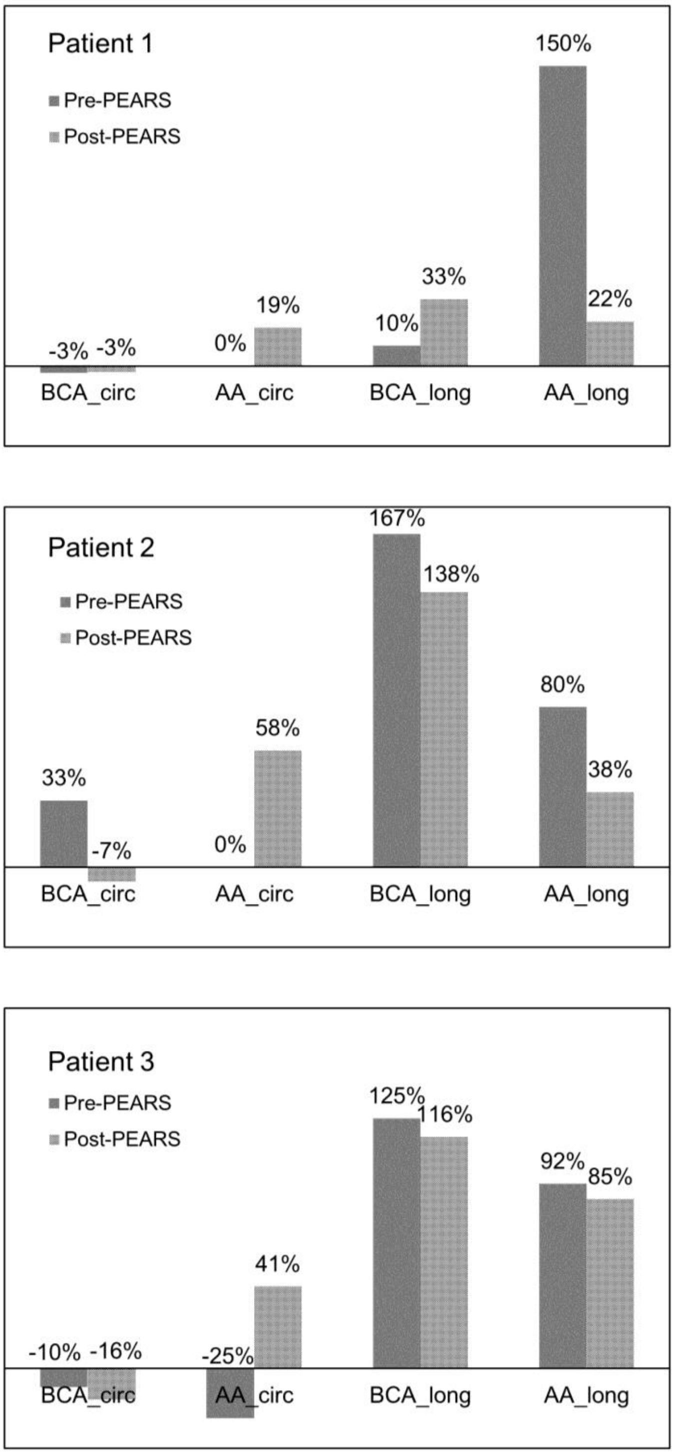

Figure 7: Percentage changes in circumferential and longitudinal wall stresses in selected regions for all models, showing the effect of aortic root motion. The percentages shown represent the increase (positive) or decrease (negative) in the wall stress *after imposing the aortic root motion boundary*. BCA_circ: circumferential stress in the region between the brachiocephalic artery and left common carotid artery; AA_circ: circumferential stress in the proximal ascending aorta; BCA_long: longitudinal stress in the region between the brachiocephalic artery and left common carotid artery; AA_long: longitudinal stress in the proximal ascending aorta

Pre-PEARS vs Post-PEARS

Figure 8 shows changes in circumferential and longitudinal stresses in regions between the BCA and LCCA and the proximal ascending aorta upon addition of the PEARS, with and without aortic root motion. Like the data analysed from Figure 7, the quantitative differences arise due to variations in patient-specific geometries and applied loading. Regardless of the effect of aortic root motion, the post-PEARS models showed qualitatively similar trends when compared to their pre-PEARS counterparts:

- Circumferential stress between the BCA and LCCA: this was increased in all patients, for models with and without aortic root motion;
- Circumferential stress in the proximal ascending aorta: there was a significant increase in Patient 2 and 3 when the root was fixed, but no appreciable changes were found when the root motion was included; Patient 1 displayed an increase in circumferential stress both with and without the aortic root motion;
- Longitudinal stress between the BCA and LCCA: In all models, this stress was increased;
- Longitudinal stress in the proximal ascending aorta: Patients 2 and 3 showed reductions in this stress both with and without the aortic root motion; Patient 1 however had an increase when the root was fixed but a reduction upon addition of the root motion.

The latter finding is of particular interest because it shows the post-PEARS models had reduced longitudinal stress in the proximal ascending aorta when compared to the pre-PEARS models.

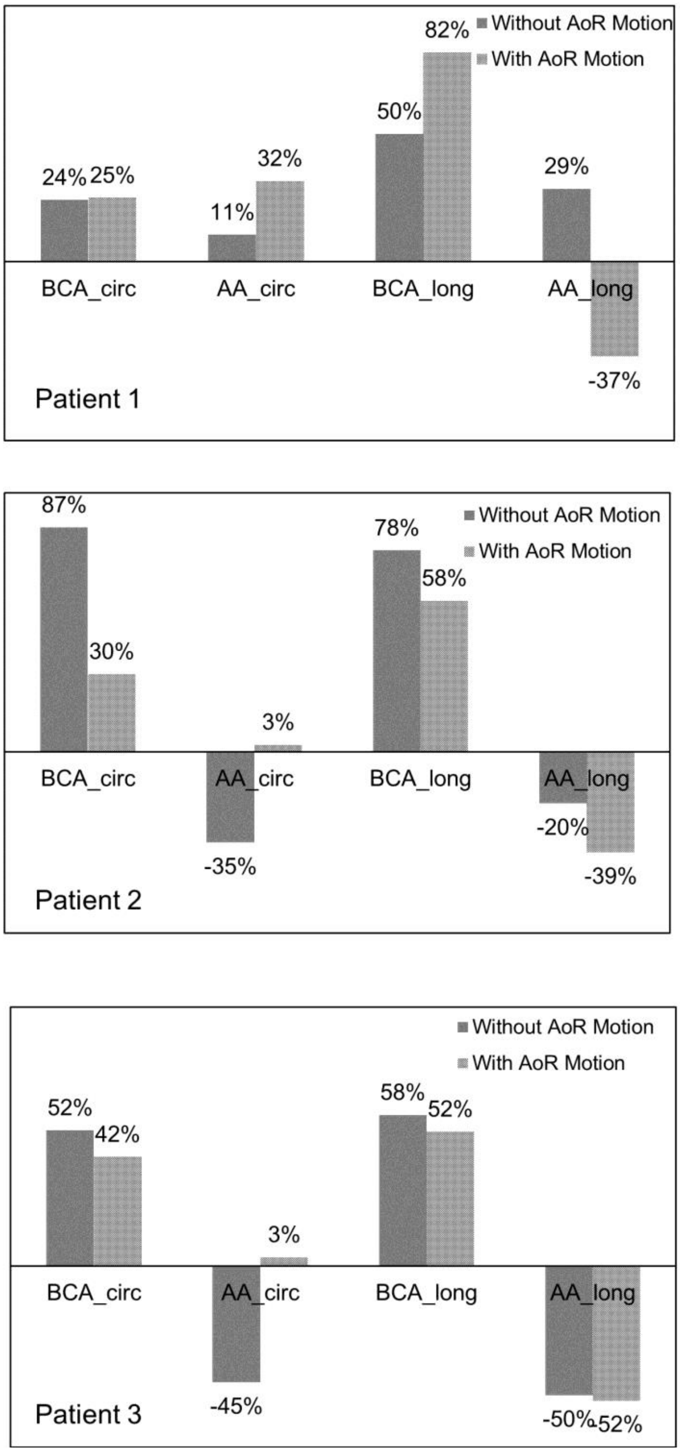

Figure 8: Percentage changes in circumferential and longitudinal wall stresses in selected regions for all models, showing the effect of PEARS. The percentages shown represent the increase (positive) or decrease (negative) in the wall stress *upon addition of PEARS*. BCA_circ: circumferential stress in the region between the brachiocephalic artery and left common carotid artery; AA_circ: circumferential stress in the proximal ascending aorta; BCA_long: longitudinal stress in the region between the brachiocephalic artery and left common carotid artery; AA_long: longitudinal stress in the proximal ascending aorta

Discussion

In a previous FE study (Singh et al., 2015), the overall stress distributions in the pre- and post-PEARS models were investigated under the assumption that the aortic root was fixed. It was observed that in the pre-PEARS models, the ascending aorta and aortic arch had higher von Mises stresses than regions distal to the aortic arch. Upon integration of PEARS into the aortic wall, the high stress regions shifted to the unsupported aortic wall, with peak stresses located at the interface between the supported and unsupported aorta. This study extends the analysis by removing the fixed root assumption and further examining the circumferential and longitudinal stresses separately.

The first major finding was the increase in aortic wall deformation upon introduction of aortic root motion. In cardiac patients, the aortic root was found to experience a downward movement ranging from 0 to 22 mm (Beller et al., 2008a). The values measured from MR images of the patients included in this study were well within this range, 13.1±5.5mm (pre-PEARS) and 10.3±2.0mm (post-PEARS). As expected, the post-PEARS aortas had reduced displacements at the aortic root and ascending aorta due to its stiffer mechanical properties. Stress analyses revealed that there were significant changes in the peak stress values when aortic root motion was included in the models. At the junction between the BCA and LCCA, there was a modest increase in the longitudinal stress for Patient 1, with a 10% increased pre-PEARS and 33% increased post-PEARS. Patients 2 and 3, however, displayed increases of 167% and 125% respectively in their pre-PEARS models and 138% and 116% respectively in their post-PEARS models. Similarly, in the ascending aorta, the longitudinal stresses increased by 150%, 80% and 92% in the pre-PEARS models of patients 1, 2 and 3, respectively, and 22%, 38% and 85% in the corresponding post-PEARS models. The effects of aortic root motion on circumferential stresses were more modest.

It has been reported that about 65 to 87% of aortic dissections occur in the ascending aorta (Hirst et al., 1958, Thubrikar et al., 1999). This, along with observations of increasing longitudinal stresses in aortic aneurysm growth, has led to the postulate that intimal tears in the circumferential direction could be explained on the basis that the tear is caused by rapidly increasing longitudinal stress on the inner surface of the aneurysm. Since aortic root motion has been directly related to increased longitudinal stress, it has been identified as an additional risk factor for aortic dissection (Beller et al., 2008b). Wrapping of the Marfan aorta with the much stiffer PEARS has an obvious additional advantage in reducing aortic root motion and ascending aorta deformation. As expected, the decreased aortic motion then resulted in reduction of longitudinal wall stress in the post-PEARS aortas (by 37-52%) when compared with their pre-PEARS counterparts. However, it also caused an increase in circumferential stress. In a multi-layer analysis of the aortic wall, Gao et al. (2006) suggested that high stress regions were typically found in the stiffer aortic layers. One of the concerns of PEARS is that the aortic wall distal to the support is unprotected and therefore susceptible to abnormal stress patterns and consequently dissection. It was shown that upon addition of PEARS, the circumferential and longitudinal stresses between the BCA and LCCA were increased by 25 to 42% and 52 to 82%, respectively. Nevertheless all peak stresses were below the known yield stress of the dilated thoracic aorta (1.18±0.12 MPa in circumferential and 1.21±0.09 MPa in longitudinal directions) (Vorp et al., 2003), with the maximum longitudinal stress predicted by the models reaching just less than half this value, and therefore did not present an imminent risk.

In addition to the limitations presented in Singh et al. (2015), this study included two additional assumptions: exclusion of the sinuses of Valsalva and simplification of the aortic root motion by neglecting its twisting. Previous studies revealed that most acute dissections of the ascending aorta were distal within the first few centimetres of the ascending aorta, and so for simplicity, the sinuses of Valsalva were neglected. Additionally, Beller et al. (2004) found that twisting of the aortic root did not appreciably change the wall stresses obtained, and was therefore neglected in these models.

Conclusions

After PEARS implantation, the axial downward motion of the aortic root was significantly reduced. Aortic root motion was previously identified as a risk factor for aortic dissection due to the corresponding increase in longitudinal stress in the ascending aorta. In this manuscript, the impact of aortic root motion on stress distribution in the Marfan aorta, pre- and post-PEARS implantation, was investigated. While the qualitative changes in stress were similar with and without aortic root motion, models incorporating aortic root motion were a step closer to a realistic description of the biomechanical environment of the aorta. It was confirmed that with the root motion, there was indeed a concentration of longitudinal wall stress in the ascending aorta of the pre-PEARS models. However, implantation of PEARS reduced this stress by up to 52% in the three patients examined in this study.

Acknowledgments

This work is supported by the NIHR Cardiovascular Biomedical Research Unit at the Royal Brompton Hospital and Imperial College London. Shelly Singh is supported by a PhD scholarship from the Government of the Republic of Trinidad and Tobago. The authors are grateful to Mr Tal Golesworthy (ExoVasc®, Exstent Ltd, Tewkesbury, UK) for his insightful discussions and suggestions.

References

BELLER, C. J., LABROSSE, M. R., HAGL, S., GEBHARD, M. M. & KARCK, M. 2008a. Aortic root motion remodeling after aortic valve replacement--implications for late aortic dissection. *Interact Cardiovasc Thorac Surg,* 7**,** 407-11.

BELLER, C. J., LABROSSE, M. R., THUBRIKAR, M. J. & ROBICSEK, F. 2004. Role of Aortic Root Motion in the Pathogenesis of Aortic Dissection. *Circulation,* 109**,** 763-769.

BELLER, C. J., LABROSSE, M. R., THUBRIKAR, M. J. & ROBICSEK, F. 2008b. Finite element modeling of the thoracic aorta: including aortic root motion to evaluate the risk of aortic dissection. *J Med Eng Technol,* 32**,** 167-70.

GAO, F., WATANABE, M. & MATSUZAWA, T. 2006. Stress analysis in a layered aortic arch model under pulsatile blood flow. *Biomedical engineering online,* 5**,** 25.

HIRST, A. E., JR., JOHNS, V. J., JR. & KIME, S. W., JR. 1958. Dissecting aneurysm of the aorta: a review of 505 cases. *Medicine (Baltimore),* 37**,** 217-79.

IZGI, C., NYKTARI, E., ALPENDURADA, F., BRUENGGER, A. S., PEPPER, J., TREASURE, T. & MOHIADDIN, R. 2015. Effect of personalized external aortic root support on aortic root motion and distension in Marfan syndrome patients. *Int J Cardiol,* 197**,** 154-60.

KOZERKE, S., SCHEIDEGGER, M. B., PEDERSEN, E. M. & BOESIGER, P. 1999. Heart motion adapted cine phase-contrast flow measurements through the aortic valve. *Magn Reson Med,* 42**,** 970-8.

NATHAN, D. P., XU, C., PLAPPERT, T., DESJARDINS, B., GORMAN, J. H., 3RD, BAVARIA, J. E., GORMAN, R. C., CHANDRAN, K. B. & JACKSON, B. M. 2011. Increased ascending aortic wall stress in patients with bicuspid aortic valves. *Annals of Thoracic Surgery,* 92**,** 1384-9.

PEPPER, J., GOLESWORTHY, T., UTLEY, M., CHAN, J., GANESHALINGAM, S., LAMPERTH, M., MOHIADDIN, R. & TREASURE, T. 2010a. Manufacturing and placing a bespoke support for the Marfan aortic root: description of the method and technical results and status at one year for the first ten patients. *Interact Cardiovasc Thorac Surg,* 10**,** 360-5.

PEPPER, J., JOHN CHAN, K., GAVINO, J., GOLESWORTHY, T., MOHIADDIN, R. & TREASURE, T. 2010b. External aortic root support for Marfan syndrome: early clinical results in the first 20 recipients with a bespoke implant. *J R Soc Med,* 103**,** 370-5.

SINGH, S. D., XU, X. Y., PEPPER, J. R., TREASURE, T. & MOHIADDIN, R. H. 2015. Biomechanical properties of the Marfan's aortic root and ascending aorta before and after personalised external aortic root support surgery. *Med Eng Phys,* 37**,** 759-66.

STUBER, M., SCHEIDEGGER, M. B., FISCHER, S. E., NAGEL, E., STEINEMANN, F., HESS, O. M. & BOESIGER, P. 1999. Alterations in the local myocardial motion pattern in patients suffering from pressure overload due to aortic stenosis. *Circulation,* 100**,** 361-8.

THUBRIKAR, M. J., AGALI, P. & ROBICSEK, F. 1999. Wall stress as a possible mechanism for the development of transverse intimal tears in aortic dissections. *J Med Eng Technol,* 23**,** 127-34.

TREASURE, T., PEPPER, J., GOLESWORTHY, T., MOHIADDIN, R. & ANDERSON, R. H. 2011. External aortic root support: NICE guidance. *Heart,* 98**,** 65-8.

VERBRUGGHE, P., VERBEKEN, E., PEPPER, J., TREASURE, T., MEYNS, B., MEURIS, B., HERIJGERS, P. & REGA, F. 2013. External aortic root support: a histological and mechanical study in sheep. *Interact Cardiovasc Thorac Surg,* 17**,** 334-9.

VORP, D. A., SCHIRO, B. J., EHRLICH, M. P., JUVONEN, T. S., ERGIN, M. A. & GRIFFITH, B. P. 2003. Effect of aneurysm on the tensile strength and biomechanical behavior of the ascending thoracic aorta. *Ann Thorac Surg*, 75**,** 1210-4.